JTTEE5 16:634–642
DOI: 10.1007/s11666-007-9082-z
1059-9630/$19.00 © ASM International

Peer Reviewed

A Three-Dimensional Analysis of the Cold Spray Process: The Effects of Substrate Location and Shape

B. Samareh and A. Dolatabadi

(Submitted March 12, 2007; in revised form July 26, 2007)

A three-dimensional model of a Cold Gas Dynamic Spray system with a peripheral nonaxisymmetric powder feeder is studied in this work. It is found that the stagnation pressure alternates for different substrate standoff distances due to the nature of the supersonic flow interaction with the substrate. One can find the optimum substrate location for any given operating condition, which results in minimum pressure buildup on the substrate. The three-dimensional analysis sheds more light on the complex gas and particle flow fields generated due to the three-dimensional particle injection process. In addition, the three-dimensional model allows us to further investigate the effect of practical substrate shapes (such as convex and concave) on the flow field and consequently to determine the optimum conditions to deposit coating particles.

Keywords cold spray process, fluid dynamics, numerical modeling, particle dynamics, shock-particle interactions

1. Introduction

The Cold Gas Dynamic Spray (CGDS) is a technology used to deposit accelerated particles on a substrate. This is a direct material deposition method that utilizes the kinetic energy of particles. In comparison to Plasma and HVOF (High Velocity Oxy-Fuel) processes, cold spray is a newly emerged thermal spray process, which can be used for fine particles typically between 1 and 60 μm at temperatures below the melting point. The coating quality is upgraded with dense layers of coating with higher bonding force and lower oxidation. The method was originally developed at the Institute of Theoretical and Applied Mechanics of the Russian Academy of Science in Novosibirsk (Ref 1).

The cold spray system is basically composed of a converging-diverging DeLaval nozzle, a powder feeder, a high-pressure gas tank and a gas heater. The compressed gas expands and accelerates in the nozzle, developing a supersonic flow in the diverging section of the nozzle. The particles are also injected into the nozzle, where they are propelled and accelerated by the gas flow. There are two different methods to introduce the particles into the nozzle. In the first method, referred as Papyrin's process (Ref 2, 3), the particles are injected into the converging section along the axis of the nozzle. In the second approach, particles are introduced downstream of the nozzle throat at an angle of 45°, where the gas pressure is lower than the ambient (Ref 4). The nozzle used in this simulation uses the second method as the powder feeder is not axisymmetric and is located after the nozzle throat.

At the exit of the nozzle, particles velocity may be as high as 800 m/s when nitrogen is used as the carrier gas. However, after particles pass through a series of diamond shocks and a strong bow shock formed on the substrate, their

This article is an invited paper selected from presentations at the 2007 International Thermal Spray Conference and has been expanded from the original presentation. It is simultaneously published in *Global Coating Solutions, Proceedings of the 2007 International Thermal Spray Conference*, Beijing, China, May 14-16, 2007, Basil R. Marple, Margaret M. Hyland, Yuk-Chiu Lau, Chang-Jiu Li, Rogerio S. Lima, and Ghislain Montavon, Ed., ASM International, Materials Park, OH, 2007.

B. Samareh and **A. Dolatabadi**, Department of Mechanical and Industrial Engineering, Concordia University, EV004.139, 1455 de Maisonneuve Blvd., Montreal, QC, Canada H3G 1M8. Contact e-mail: dolat@encs.concordia.ca.

Nomenclature	
A	Cross-sectional area of the particle, m^2
C_D	Drag coefficient
D	Particle diameter, m
F_b	Body force, N
Ma	Mach number
m	Mass, kg
R	Specific gas constant, J/kg K
Re	Reynolds number
T	Temperature, K
t	Time, s
$\boldsymbol{V}$	Velocity vector, m/s
ρ	Density, kg/m^3
γ	Specific heat ratio
μ	Molecular viscosity, kg/m s
Subscript	
p	Particle
g	Gas

velocities decrease drastically. The deposition efficiency is usually around 50% as some of the particles are washed away because of the presence of high velocity and high pressure regions near the substrate. Also, some of them can bounce off the substrate and escape into the surrounding environment. Only those particles with a velocity larger than a critical velocity (Ref 5) can successfully be deposited on the substrate. Deposition efficiency is highly related to the particle material and size distribution as well as the flow field parameters.

One of the parameters that can improve the efficiency is the particle normal velocity upon impact on the substrate. This in turn, is influenced by the nozzle geometry, stagnation temperature and pressure of the gas, particle material, gas species, particle size and substrate location and geometry. Many experiments and simulations have been done to study the effect of the particle size and spray angle (Ref 5) as well as the substrate geometry and location in two-dimensional (Ref 6). Power et al. (Ref 7) and Smith et al. (Ref 8) modeled the flow field of a sonic nozzle. In this study, internal and external flow fields where solved separately due to the choked flow inside the nozzle. A one-way Lagrangian scheme was also used to model the interactions between the gas and solid phases. Similar studies were also performed by Oberkampf and Talpallikar (Ref 9, 10), Yang and Eidelman (Ref 11), Hassan et al. (Ref 12) and Dolatabadi et al. (Ref 13-15).

In this numerical study, however, due to the orientation and location of the particle feeder, which is placed on the periphery of the nozzle throat, and the substrate shape, a two-dimensional simulation is not adequate to reveal all of the aspects of the flow field and particles trajectory. Therefore, a complete three-dimensional analysis using Fluent 6.2.16 is conducted to find the effect of the substrate geometry. The focus is also on the interactions of the shock diamonds and the bow shock formed on the substrate which results in different stagnation pressures at different standoff distances. As this variation is not linear and the pressure alternates with location, an optimum standoff distance can be identified to obtain the best particle velocity distribution upon impact on a substrate.

2. Numerical Methodology

2.1 Geometry

A schematic of the CGDS system is presented in Fig. 1. Two different substrate shapes (flat and cylindrical) with different standoff distances are modeled in order to investigate the effect of substrate geometry on the flow field and particle deposition.

The nozzle has a circular cross section with an inlet diameter of 8 mm. The converging section has a length of 50 mm and is attached to the throat section with a diameter of 4 mm and a length of 30 mm. It then expands to a diameter of 6 mm located at a distance of 97 mm from the throat end. The particle feeder is placed at the beginning of the throat and injects particles at an angle of 45° with respect to the nozzle axis. Flat substrates are square plates having a side length, h, of 20 mm, placed at standoff distances, d, of 7.5, 10, 12.5, 15, 17.5, and 20 mm. Another case with a cylinder having a diameter of 4 mm is also modeled to see the effect of a substrate with a small radius of curvature on the flow field.

In all these cases, boundaries are extended in such a way that the independency of the solution on the computational domain is guaranteed. The orientation of the particle feeder and substrates will allow having a plane of symmetry, which will reduce the computational time considerably.

2.2 Computational Domain

A hybrid scheme is used to generate hexahedral and tetrahedral elements throughout the domain. Hexahedral cells are the dominant elements (being more that 80% of the total number of cells), while tetrahedral elements are adapted to the regions where the hexahedral scheme is not suitable and will result in high skewness and aspect ratio. In order to avoid wedged elements at the nozzle centerline, another sub-mesh is used in this region. This ensures a higher grid quality and more accurate results. The total grid size varies between 170,560 and 923,960 cells depending on the substrate shape, location and size. A grid dependency study is also done to ensure that the solution dependency on the grid will be less than 2%. A cross section of the grid for a flat substrate with a height of 20 mm located at a standoff distance of 20 mm is shown in Fig. 2 with a close-up view of the sub-mesh zone.

2.3 Gas Phase

The ideal gas law is used to calculate density, in order to have the compressibility effects taken into account. Since the flow is high speed and compressible, viscosity changes with temperature become important. In order to account for this effect, three coefficients Sutherland viscosity law is used, which is specially suggested for high

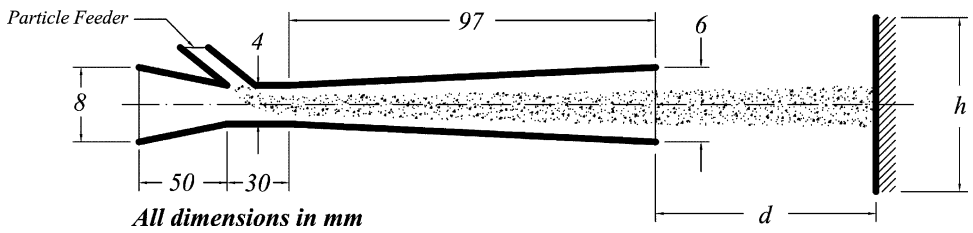

Fig. 1 Schematic of the nozzle and the substrate (not to scale)

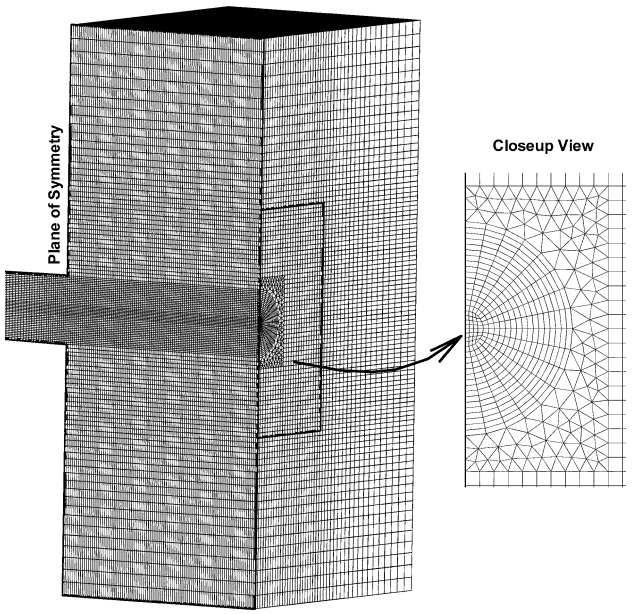

Fig. 2 Cross section of the grid for a flat substrate located at a standoff distance of 20 mm

speed compressible flows (Ref 16). Due to the presence of diamond shocks at the nozzle exit and bow shock on the substrate, the flow will experience sharp gradients and steep changes in pressure and velocity. Therefore, the RSM (Reynolds Stress Model) turbulence model is used in this simulation as it takes into account the compressibility effect as well as streamline curvature, swirl, rotation, and rapid changes in strain rate in a more rigorous manner compared to other models and will result in higher accuracy (Ref 16-18). However, as this method creates a high degree of coupling between the momentum equation and the turbulence stresses in the flow, calculations can be more susceptible to stability and convergence difficulties compared to the k-ε model (Ref 16). In order to overcome this problem, for each case, the calculation begins with the k-ε model with low under-relaxation factors, and is then switched to the RSM scheme. The segregated implicit solver with second order accuracy for pressure terms and QUICK discretization scheme for momentum and density is used. For compressible flows with shocks, the first order upwind scheme may tend to smooth the shocks, hence using the QUICK scheme for density and momentum is highly recommended for hexahedral grids (Ref 16, 19).

2.4 Particle-Fluid Interaction

A Lagrangian approach is used to obtain particle trajectories. Tracking particles in a Lagrangian frame requires the second phase to be dilute enough so that the particle-particle interactions and the effect of the particles on the gas phase can be neglected. This assumption requires the second phase to have a low volume fraction (Ref 20-24). The velocity of the particles in the field can be obtained by integrating Eq 1.

$$m_p \frac{dV_p}{dt} = C_D \rho_g (V_g - V_p)(|V_g - V_p|) \frac{A_p}{2} + F_b \qquad \text{(Eq 1)}$$

The particle position can be derived by further integration of this equation over time (Ref 25). Particle deceleration due to the adverse pressure gradient caused by the bow shock is taken into account as the body force in Eq 1. The body force per unit particle mass can be represented as:

$$F_b = \left(\frac{\rho}{\rho_p}\right) V_p \cdot \nabla V_g \qquad \text{(Eq 2)}$$

Drag coefficient: One of the important factors which has a significant influence on the accuracy of the predicted particle velocity is the drag coefficient. C_D is a strong function of the particle Reynolds and Mach number, Re_p and Ma_p, and can be determined using the relative velocity of the particles with respect to the fluid. Re_p and Ma_p are defined as:

$$Re_p = \frac{\rho_g |V_g - V_p| D}{\mu_g} \qquad \text{(Eq 3)}$$

$$Ma_p = \frac{|V_g - V_p|}{\sqrt{\gamma\, RT_g}} \qquad \text{(Eq 4)}$$

A correlation is proposed by Crowe (Ref 26) that accounts for a large range of particle Mach numbers and Reynolds numbers ($0.1 < Ma_p < 2$ and $0.2 < Re_p < 10^4$). This range is sufficient for a typical CGDS process and will accommodate all the conditions encountered inside the flow field. The equation proposed by Crowe is:

$$C_D = (C_{D(inc)} - 2)\, e^{-3.07\gamma^{1/2}\left(\frac{Ma_p}{Re_p}\right) g(Re_p)} + \frac{h(Ma_p)}{\gamma^{1/2} Ma_p} e^{\frac{-Re_p}{2Ma_p}} + 2 \qquad \text{(Eq 5)}$$

where $C_{D(inc)}$ is the drag coefficient for a sphere in incompressible flow, and $g(Re_p)$ and $h(Ma_p)$ are the devised functional relations

$$\log_{10} g(Re_p) = 1.25\left[1 + \tanh\left(0.77 \log_{10} Re_p - 1.92\right)\right] \qquad \text{(Eq 6)}$$

$$h(Ma_p) = \left\{2.3 + 1.7\left[T_p/T_g\right]^{1/2}\right\} - 2.3 \tanh(1.17 \log_{10} Ma_p) \qquad \text{(Eq 7)}$$

The drag coefficient for a sphere in an incompressible gas is taken from a correlation by Clift et al. (Ref 27).

2.5 Boundary Conditions

The nozzle inlet is modeled as a mass flow inlet due to a better convergence rate compared to a pressure inlet. By having an inlet pressure of 0.62 MPa and a total temperature of 773 K and assuming that the Mach number at the throat is unity, the mass flow rate through the nozzle will be 0.011 kg/s. This mass flow rate will result in a pressure

of 0.62 MPa upstream of the nozzle. The flow velocity is negligible at the inlet and therefore, the total and static pressure and temperature are equal. The direction of the velocity vector at the inlet is assumed to be perpendicular to this boundary. The turbulence intensity is 1% and the length scale is set to be 20% of the nozzle diameter at the throat, as proposed previously (Ref 28).

The effect of heat transfer through the nozzle wall is negligible and it is assumed that the nozzle wall has a constant temperature of 300 K, which is equal to the ambient temperature. The substrate wall is assumed to have a negligible heat transfer to the surrounding ambient, and is considered to be adiabatic. Surrounding boundaries are assumed to be pressure outlets as they are far enough to have no effect on the solution. Pressure on these boundaries is set to be atmospheric.

Particle injection: More than 5000 particles are used to obtain reliable statistical data. The projected area of the particle feeder on the nozzle wall is used as the inlet boundary for the particles. In order to resemble the stochastic behavior the particles inside the flow field, they are injected in a complete random order. A MATLAB (The MathWorks Inc.) code is developed to simulate this process. The particle size distribution used in this simulation is shown in Table 1. Particle diameters are selected randomly in each size range in such a way that they resemble the given distribution. Then, a random initial position inside the projected area will be associated with each particle. Finally, an initial velocity between 15 and 25 m/s at an angle between 40 and 50 degrees with respect to the nozzle axis will be selected randomly for injection.

3. Results and Discussions

The gas phase pressure and Mach number iso-surfaces are shown in Fig. 3(a) and (b), respectively. Because of the strong bow shock formed on the substrate, a high stagnation pressure zone is created near the plate. This high pressure region will result in a deceleration of the particles as well as off-normal impact on the substrate. The deviation of particle trajectories from the centerline can be so strong that some particles may not impact the substrate and are washed away by the gas flow. Additionally, those particles that hit the substrate with such a low-normal impact velocity cannot make a strong bond to the plate and will slide down. These two phenomena are found to be directly responsible to reduce the process deposition efficiency.

Table 1 Particles size distribution

> Diameter, μm	% Volume
20	7
30	23
40	40
50	65
60	100

Static pressure and Mach number versus the distance from the nozzle exit for a flat substrate located at different standoff distances are shown in Fig. 4(a) and (b). A case without the substrate is also modeled to see the effect of the substrate on the shocks. It can be observed that as the gas passes through several diamond shocks, which are composed of a series of compression waves and Prandtl-Meyer expansion waves, its kinetic energy dissipates gradually until the pressure reaches the surrounding pressure. Placing a substrate in front of this free jet will result in a pressure rise on the substrate. In a subsonic flow regime, the peak pressure rise will decrease by increasing the substrate distance from the nozzle exit. However, for supersonic flows, due to the compression and expansion waves, the peak pressure alternates by changing the location of the substrate. Pressure rise up begins at a small distance from the plate where the flow starts to feel the presence of the substrate. The value of the maximum pressure peak depends on the location where the pressure starts to increase. The minimum value of 330 kPa can be achieved by placing the substrate at a distance which results in a pressure rise starting in a pressure valley. Referring to this figure, this situation corresponds to the case with a standoff distance of approximately 10 mm.

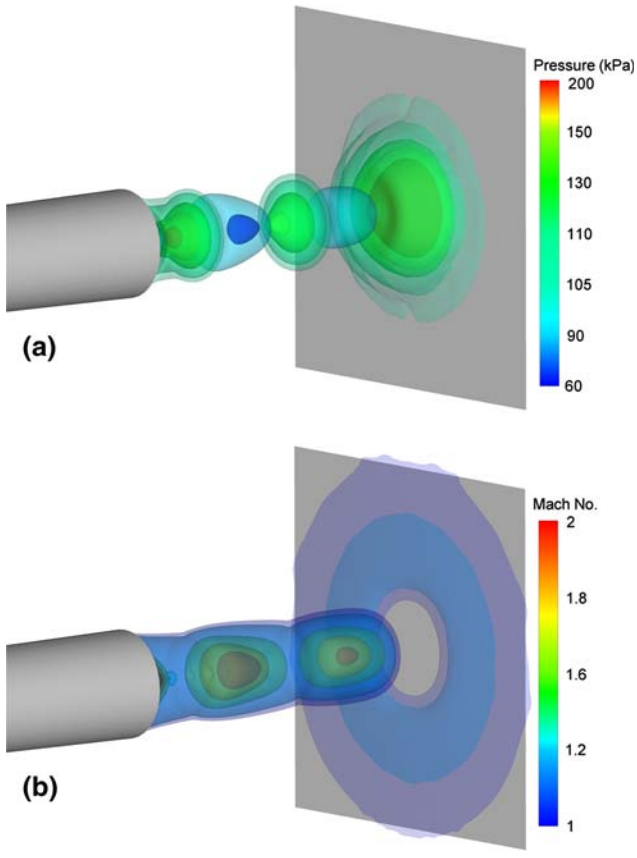

Fig. 3 (a) Pressure iso-surfaces for a flat substrate located at a standoff distance of 20 mm. (b) Mach number iso-surfaces for the same substrate

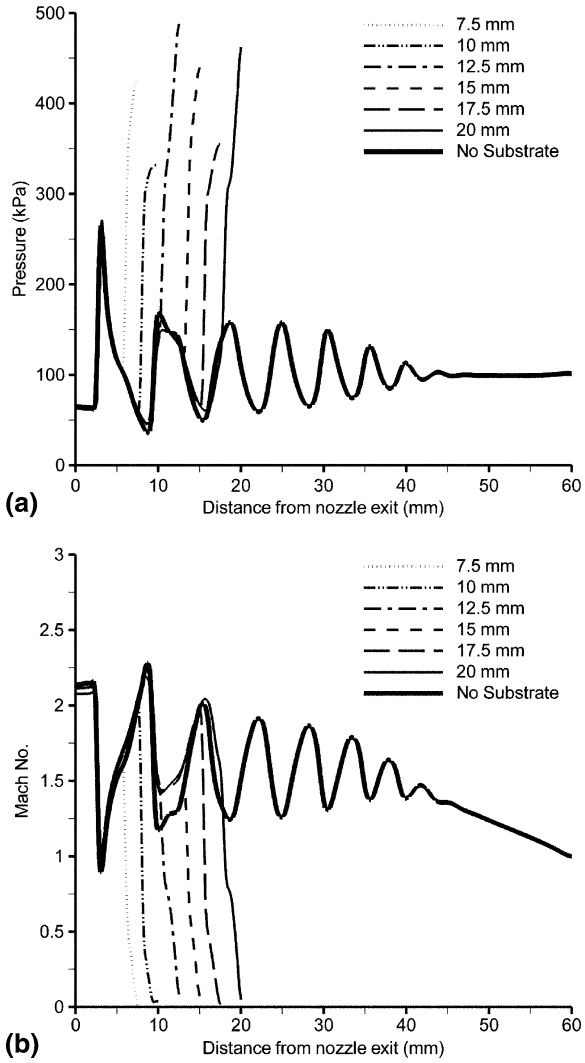

Fig. 4 (a) Pressure variations along the centerline for various standoff distances for a flat square substrate. (b) Mach number variations along the centerline for various standoff distances for the same substrate

The location of the substrate is of great importance as it determines the landing situation for the particles. A high stagnation pressure region on the substrate decelerates particles before hitting the substrate and results in a lower deposition efficiency. On the other hand, having a low pressure region before the substrate will result in higher impact velocity, lower dispersion and consequently, higher deposition efficiency. In this study, it is observed that placing the substrate at a distance of 10 mm from the nozzle exit will result in the lowest peak pressure. So, the upcoming results will be presented for this optimum case.

The gas pressure and Mach number iso-surfaces for the case with a cylindrical substrate having a diameter of 4 mm located at 10 mm from nozzle exit are shown in Fig. 5(a) and (b), respectively. Due to the supersonic gas leaving the nozzle, the flow pattern is the same as that of a flat plate except for the region near the substrate where the flow starts to sense the presence of the cylinder.

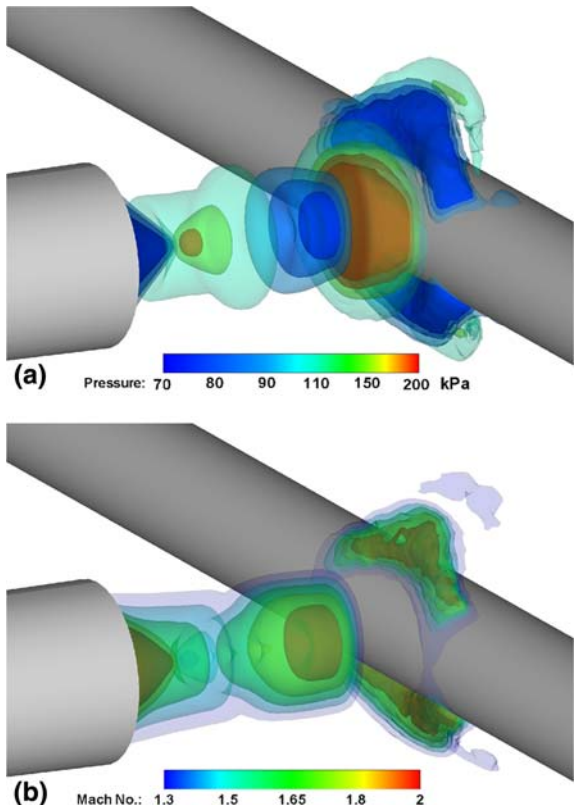

Fig. 5 (a) Pressure iso-surfaces for a cylindrical substrate with a diameter of 4 mm located at a standoff distance of 10 mm. (b) Mach number iso-surfaces for the same substrate

Similarly, the bow shock is formed on the substrate due to the high velocity gas coming to rest on the cylinder's front. The strength of this bow shock is expected to be less in comparison to the case with the flat substrate as the flow is not fully blocked and is allowed to pass over the cylinder. On the other hand, because of the substrate geometry and the resultant flow pattern, coating particles will have a lower chance to hit the substrate and tend to escape the field. In contrast to the flat substrate case, the particles impinging on the cylinder will also attain lower normal impact velocity due to the radius of curvature of the substrate. These phenomena will have a negative effect on the coating deposition efficiency and quality when using the cylindrical substrate.

Figure 6 shows the footprint of the particles at a distance of 10 mm from the nozzle exit when there is no substrate blocking the high speed jet. The landing location for a range of particle sizes varying between 5 and 60 μm, impinging on a flat square substrate located at a standoff distance of 10 mm is shown in Fig. 7. Particles deviation in both vertical and lateral directions which is due to the three-dimensional nature of the flow is shown in this figure. Smaller particles, having low Stokes numbers, are more affected by the gas flow and are deviated more compared to the heavy ones. Particles are injected from the top side of the nozzle at random angles between 40 and 50 degrees. As the heavier particles are less affected

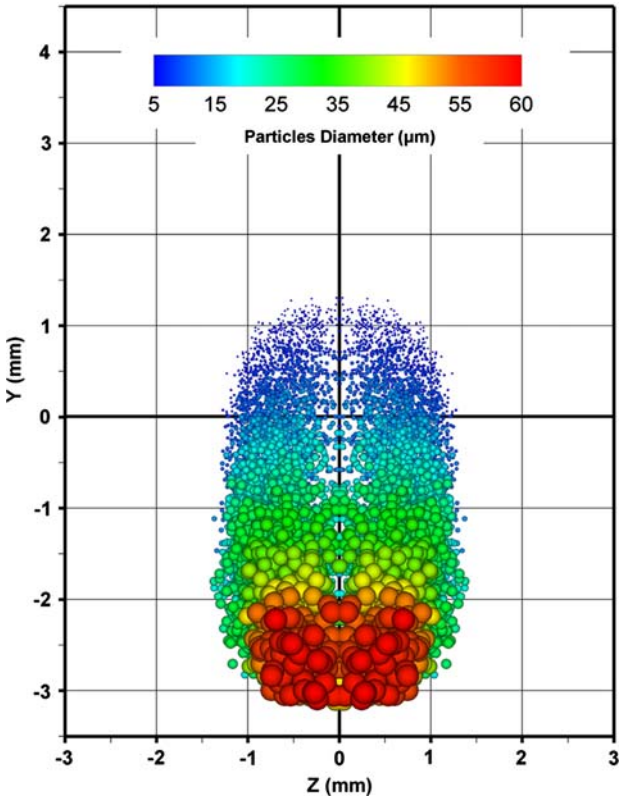

Fig. 6 Footprint of a particle range between 5 and 60 μm at a distance of 10 mm from nozzle exit when there is no substrate blocking the free jet

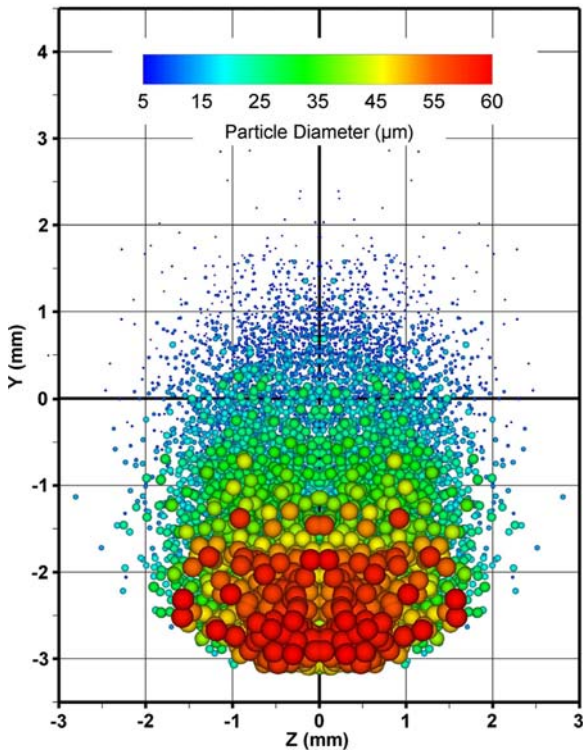

Fig. 7 Landing location for a particle range between 5 and 60 μm for a flat substrate, placed at a standoff distance of 10 mm

by the flow, they shift below the nozzle centerline while the smaller particles are dispersed above and below the centerline. The landing locations for the same particle size distribution hitting the cylindrical substrate are shown in Fig. 8. It can be seen that the particles dispersion is less for the cylindrical substrate than for the flat substrate, and is minimum when there is no substrate. This is due to the strength of the bow shock formed on the substrate. For the cylindrical case, the shape of the substrate will result in a weaker bow shock as the flow is not fully blocked and is able to pass over the cylinder, while the flat substrate will result in the highest level of particle dispersion due to the formation of a stronger bow shock. Referring to Fig. 8, it can be seen that most of the heavy particles (shown in grey) that are moving below the center line, fall out of the projected area of the substrate and pass the cylinder without even hitting it. On the other hand, particles hitting this substrate will attain a relatively low normal impact velocity due to the radius of curvature of the cylinder.

The variations in particles normal impact velocity versus particle size for the free jet, flat and cylindrical substrates are shown in Fig. 9(a-c), respectively. From this figure and Fig. 6 through 8, it is noticeable that smaller particles have higher velocities with more dispersion, while heavier particles travel at lower velocities and are dispersed less. Another phenomenon which is quite visible in Fig. 9 is the velocity standard deviation for different

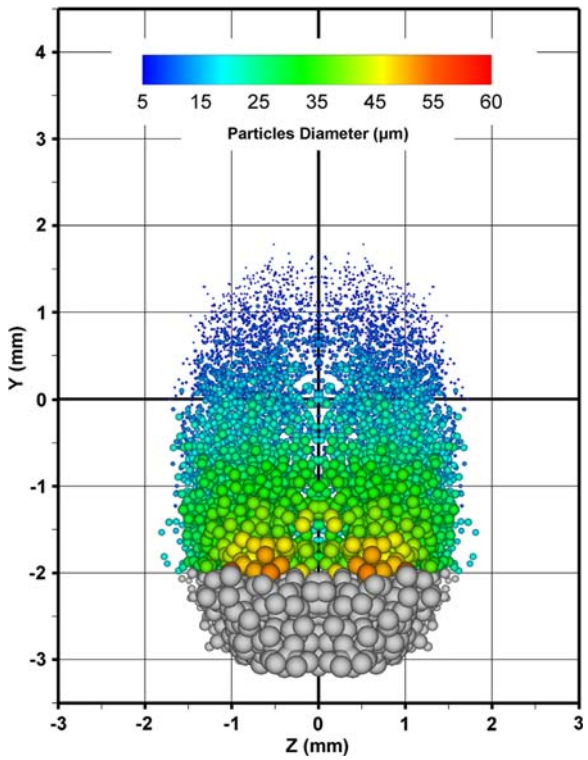

Fig. 8 Landing location for a particle range between 5 and 60 μm for a cylindrical substrate with a diameter of 4 mm, placed at a standoff distance of 10 mm

size ranges. The large velocity variation for heavy particles observed in these figures is due to the variation in injection angle and velocity. Because of the large Stokes number associated with heavy particles, the effect of the injection condition imposed on these particles will not be compensated by the gas speed as they travel the length of the nozzle. As a result, a larger velocity band width can be expected at the coating location for large particles. Figure 9(a) and (b) can be compared to study the effect of the bow shock on the particles. It is noticeable that small particles (approximately below 25 μm) are more affected by the bow shock, while the deceleration of the larger particles is almost negligible. Referring to Fig. 9(c), it can be seen that there exists a greater variation in the normal impact velocity on the cylinder which is due to the curvature of the substrate. In addition, due to the size of the substrate and the injection angle, all the particles with a diameter greater than 55 μm will not impinge on the substrate. The average normal impact velocity for various particle sizes is shown in Fig. 10. In comparing the free jet case and the case with the flat substrate, it is quite visible that the particles greater than 25 μm travel at almost the same velocity and are not affected by the bow shock formed on the flat substrate. Average normal impact velocities for the cylinder are also lower compared to the other cases as a result of the shape of the substrate. In addition, the statistical data of the landing location and impact velocity for the flat substrate are also presented in Table 2. Since all the Z values will be zero if the whole

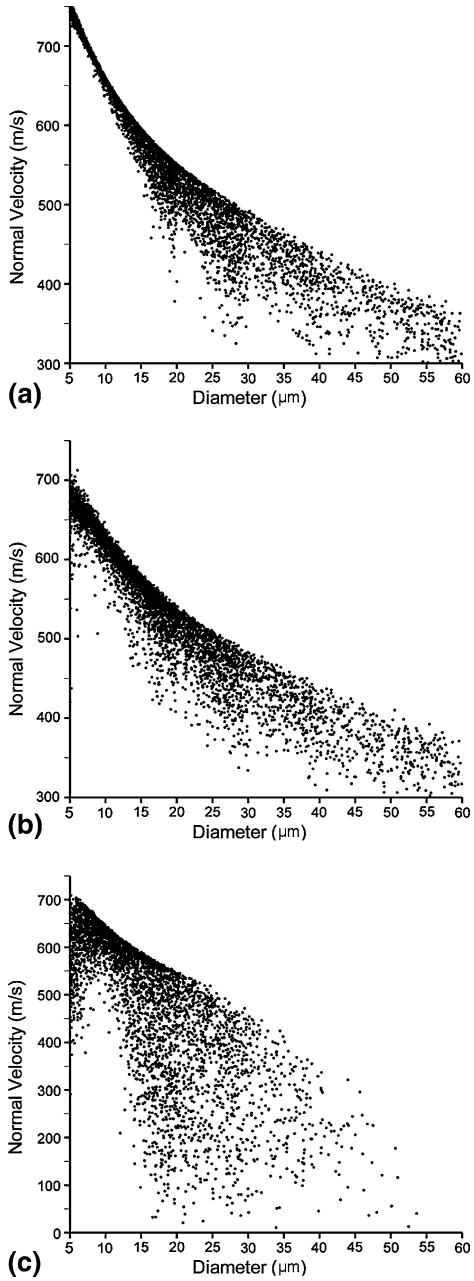

Fig. 9 Normal impact velocity versus particle size for (a) free jet case, (b) flat substrate placed at a standoff distance of 10 mm, (c) a cylindrical substrate with a diameter of 4 mm, placed at a standoff distance of 10 mm

Table 2 Statistical data of the landing location and normal impact velocity on the flat substrate (Data in the Z direction are calculated for the half of the substrate)

	Mean value			Standard deviation		
Size range, μm	Y, mm	Z, mm	Velocity, m/s	Y, mm	Z, mm	Velocity, m/s
5-10	0.323	0.729	647.647	0.741	0.496	24.623
10-15	−0.550	0.753	589.166	0.802	0.478	24.955
15-20	−1.143	0.765	533.107	0.775	0.468	29.120
20-25	−1.425	0.760	494.401	0.686	0.448	28.558
25-30	−1.749	0.749	455.946	0.674	0.435	33.109
30-35	−1.875	0.602	437.170	0.605	0.370	28.344
35-40	−2.097	0.607	410.068	0.513	0.377	28.531
40-45	−2.260	0.555	387.689	0.527	0.342	29.318
45-50	−2.366	0.603	369.479	0.412	0.386	25.835
50-55	−2.438	0.585	354.746	0.400	0.343	23.248
55-60	−2.489	0.498	344.107	0.380	0.321	22.282

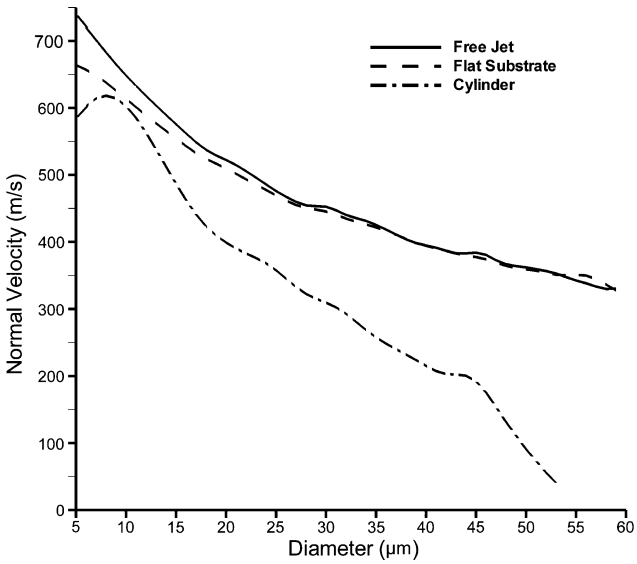

Fig. 10 Average normal impact velocity for different size ranges for the three cases studied

domain is considered, the tabulated Z values are extracted from the data of the half of the domain.

4. Conclusions

In this work, the effect of the presence of the substrate in the high-speed gas flow field outside a low-pressure cold spray nozzle is analyzed. Due to the peripheral injection of the coating powders, a three dimensional simulation was conducted to capture all the important features of the particulate phase such as the landing location on the substrate, vertical and lateral dispersion, as well as the normal impact velocity for different substrate shapes. It is found that the presence of the substrate and its standoff distance and shape have significant effects on the gas flow field near the particle deposition area. This is due to the nature of the supersonic gas flow which generates compression and expansion waves. In order to find the optimum standoff distance of the substrate, the interactions between the shock diamonds and the bow shock formed on the substrate should be analyzed carefully. In this study for the given operating conditions, the optimum location for the substrate which results in a minimum stagnation pressure of 330 kPa is found to be 10 mm from the nozzle exit. The location of the substrate will also affect the particles normal impact velocity and the vertical and lateral dispersions. Particles deviate less from their path in the case with a cylindrical substrate as the bow shock near the substrate is weaker in comparison to the flat plate. On the other hand, due to the radius of curvature of the cylinder, particles will have lower normal impact velocity, and hence their deposition will be harder to achieve and the coating quality is expected to be lower. In terms of the bow shock and particles interactions, it is observed that smaller particles (with sizes less than 25 μm) are most affected by the high pressure gradients and shocks.

Acknowledgments

The authors would like to thank Drs. E. Irissou and C. Moreau from National Research Council Canada-Industrial Materials Institute (NRC-IMI) for their technical support. This work was financially supported by the Natural Sciences and Engineering Research Council Canada (NSERC) and Le Fonds québécois de la recherche sur la nature et les technologies (FQRNT).

References

1. A.P. Alkhimov, V.F. Kosareve, and A.N. Papyrin, A Method of Cold Gas Dynamic Spray Deposition, *Dokl. Akad. Nauk SSSR*, 1990, **315**(5), p 1062-1065
2. A.P. Alkhimov, A.N. Papyrin, V.F. Kosarev, N.I. Nesterovich, and M.M. Shushapanov, Gas Dynamic Spray Method for Applying a Coating, U.S. Patent 5,302,414, 1994
3. A.P. Alkhimov, A.N. Papyrin, V.F. Kosarev, N.I. Nesterovich, and M.M. Shushapanov, Method and Device for Coating, European Patent 0 484 533 B1, 1995
4. M. Karimi, A. Fartaj, G.W. Rankin, D. Vanderzwet, J. Villafuerte, and W. Birtch, Numerical Simulation of the Cold Gas Dynamic Spray Process, *J. Thermal Spray Technol.*, 2006, **15**(4), p 518-523
5. T. Stoltenhoff and H. Kreye, Cold Spraying—from Thermal Spraying to High Kinetic Energy Spraying, *5th HVOF. Colloquium Proc.*, November 16-17, 2000 (Erding, Germany), GTS E.V. 2000
6. Q. Zhu and A. Dolatabadi, Computational Modeling of Cold Spray Process: Effect of Substrate and Particle Size on Gas-Particle Flow, *Building on 100 Years of Success: Proceedings of the 2006 International Thermal Spray Conference*, B.R. Marple, M.M. Hyland, Y.C. Lau, R.S. Lima, and J. Voyer, Eds., May 15-18, 2006 (Seattle, WA, USA), ASM International, 2006
7. G.D. Power, E.B. Smith, T.J. Barber, and L.M. Chiappetta, Analysis of a Combustion (HVOF) Spray Deposition Gun, Report 91-8, United Technologies Research Center, East Hartford, CT, 1991
8. E.B. Smith, G.D. Power, T.J. Barber, and L.M. Chiappetta, Application of Computational Fluid Dynamics to the HVOF Thermal Spray Gun, *Thermal Spray: International Advances in Coatings Technology*, C.C. Berndt, Ed., May 25-June 5, 1992 (Orlando, FL), ASM International, 1992, p 805-810
9. W.L. Oberkampf and M. Talpallikar, Analysis of a High Velocity Oxy-Fuel (HVOF) Thermal Spray Torch, Part 1: Numerical Formulation, *J. Thermal Spray Technol.*, 1996, **5**(1), p 53-61
10. W.L. Oberkampf and M. Talpallikar, Analysis of a High Velocity Oxy-Fuel (HVOF) Thermal Spray Torch, Part 2: Numerical Formulation, *J. Thermal Spray Technol.*, 1996, **5**(1), p 62-81
11. X. Yang and S. Eidelman, Numerical Analysis of a High Velocity Oxy-Fuel Thermal Spray System, *J. Thermal Spray Technol.*, 1996, **5**(2), p 175-184
12. B. Hassan, A.R. Lopez, and W.L. Oberkampf, Computational Analysis of a Three-Dimensional High Velocity Oxygen Fuel (HVOF) Thermal Spray Torch, *J. Thermal Spray Technol.*, 1998, **7**(1), p 71-77
13. A. Dolatabadi, J. Mostaghimi, and M. Ivanovic, Numerical Modeling of Particle Laden Flow in HVOF Torch with Gas Shroud, *Proceedings of the 1st International Thermal Spray Conference*, Montreal, Quebec, Canada, 2000, p 105-113
14. A. Dolatabadi, J. Mostaghimi, and M. Ivanovic, Modeling all Speed Particle Laden Flows Using a Fully Eulerian Approach, *Proceedings of the 9th Annual Conference of the CFD Society of Canada*, Waterloo, Ontario, Canada, 2001, p 412-417
15. A. Dolatabadi, J. Mostaghimi, and V. Pershin, Modeling Dense Suspension of Solid Particles in Highly Compressible Flows, *Int. J. Comput. Fluid Dyn.*, 2004, **18**(2), p 125-131
16. Fluent 6.2 User's Guide, Fluent Inc.
17. S. Sarkar, G. Erlebacher, M.Y. Hussaini, and H.O. Kreiss, Analysis and Modeling of Dilatation Terms in Compressible Turbulence, *J. Fluid Mech.*, 1991, **227**, p 473-493
18. S. Sarkar and B. Lakshmanan, Application of a Reynolds Stress Turbulence Model to the Compressible Shear Layer, *J. AIAA*, 1991, **29**(5), p 743-749
19. B. Jodoin, Cold Spray Nozzle Mach Number Limitations, *J. Therm. Spray Technol.*, 2002, **11**(4), p 496-507
20. R.C. Dykhuizen and M.F. Smith, Gas Dynamic Principles of Cold Spray, *J. Therm. Spray Technol.*, 1998, **7**(2), p 205-212
21. M. Karimi, An Investigation of the Cold Gas Dynamic Supersonic Spray Process Particle/Flow Field, MASc. Thesis, University of Windsor, Windsor, Canada, 2005
22. M. Grujicic, C. Tong, W.S. DeRosset, and D. Helfritch, Flow Analysis and Nozzle-Shape Optimization for the Cold Gas Dynamic Spray Process, *Proceedings of the Institution of Mechanical Engineers, Part B: J. Eng. Manufacture*, 2003 (London, UK), Mechanical Engineering Publications, **217**(11), p 1603-1614
23. V. Shukla, G.S. Elliott, and B.H. Kear, Nanopowder Deposition by Supersonic Rectangular Jet Impingement, *J. Therm. Spray Technol.*, 2000, **9**(3), p 394-398
24. P.H. Shipway and I.M. Hutchings, Method for Optimizing the Particle Flux in Erosion Testing with a Gas-Blast Apparatus, *Wear*, 1994, **174**(1-2), p 169-175

25. A. Dolatabadi, J. Mostaghimi, and V. Pershin, Effect of Cylindrical Shroud on Particle in High Velocity Oxy-Fuel Spray Process, *Sci. Technol. Adv. Mat.*, 2002, **3**, p 245-255
26. C.T. Crowe, Drag Coefficient on Particles in a Rocket Nozzle, *J. AIAA*, 1967, **5**(5), p 1021-1022
27. R. Clift, J.R. Grace, and M.E. Weber, Bubbles, Drops and Particles. Academic Press, New York, 1978
28. M. Karimi, G.W. Rankin, and A. Fartaj, A Numerical Investigation of the Flow Field of a Supersonic Jet Impinging on a Flat Plat, *Proceedings of the CFD Society of Canada*, 2005 (St. Johns, Newfoundland, Canada)